

# We are IntechOpen, the world's leading publisher of Open Access books Built by scientists, for scientists

6,900

Open access books available

186,000

International authors and editors

200M

Downloads

Our authors are among the

154

Countries delivered to

TOP 1%

most cited scientists

12.2%

Contributors from top 500 universities



WEB OF SCIENCE™

Selection of our books indexed in the Book Citation Index  
in Web of Science™ Core Collection (BKCI)

Interested in publishing with us?  
Contact [book.department@intechopen.com](mailto:book.department@intechopen.com)

Numbers displayed above are based on latest data collected.  
For more information visit [www.intechopen.com](http://www.intechopen.com)



---

# Parameter Recognition of Engineering Constants of CLSMs in Civil Engineering Using Artificial Neural Networks

---

Li-Jeng Huang

Additional information is available at the end of the chapter

<http://dx.doi.org/10.5772/intechopen.71538>

---

## Abstract

Controlled low-strength materials (CLSMs) had been widely applied to excavation and backfill in civil engineering. However, the engineering properties of CLSM in these embankments vary dramatically due to different contents involved. This study is proposed to employ the ANSYS software and two different artificial neural networks (ANNs), that is, back-propagation artificial neural network (BPANN) and radial basis function neural network (RBFNN), to determine the engineering properties of CLSM by considering an inverse problem in which elastic modulus and the Poisson's ratio can be identified from inputting displacements and stress measurements. The PLANE42 element of ANSYS was first used to investigate a 2D problem of a retaining wall with embankment, with  $E = 0.02\sim 3 \text{ GPa}$ ,  $\nu = 0.1\sim 0.4$  to obtain totally 270 sampling data for two earth pressures and two top surface settlements of embankment. These data are randomly divided into training and testing set for ANNs. Practical cases of three kinds of backfilled materials, soil, and two kinds of CLSMs (CLSM-B80/30% and CLSM-B130/30%) will be used to check the validity of ANN prediction results. Results showed that maximal errors of CLSM elastic parameters identified by well-trained ANNs can be within 6%.

**Keywords:** ANNs, ANSYS, CLSM, fem, parameter recognition

---

## 1. Introduction

In recent years, sustainable materials have been widely studied and developed especially for construction, highway, and civil engineering. Controlled low-strength material (CLSM) is commonly used as backfilled materials. It would be a friendly environment-cheap material and typically consists of small amount of cement, supplementary, fine aggregates, and a large amount of mixing water. Self-compacting/self-leveling, significantly low strength, as well as almost no measured settlement after hardening are remarkable characteristics of CLSM.

CLSM can be defined as a kind of self-compacting cementitious material that is in a flowable state at the initial period of placement and has specified compressive strength of 1200 *psi* (8.27 *MPa*) (or less at 28 days) or is defined as excavatable if the compressive strength is 300 *psi* (2.07 *MPa*) (or less at 28 days) [1]. Recent studies have reported that the maximum CLSM strength of approximately up to 1.4 *MPa* is suitable for most of backfilling applications when re-excavation is required [2, 3] It is also recommended that depending upon the availability and project requirements, any recycle material would be acceptable in the production of CLSM with prior tests its feasibility before uses [4]. The special features of CLSM can be summarized as follows: durable, excavatable, erosion-resistant, self-leveling, rapid curing, flowable around confined spacing, wasting material usage, elimination of compaction labors and equipment, and so on.

There are several studies on the engineering properties of CLSMs by laboratory experiments [5–10], and numerical analyses of applications of CLSM to civil engineering, such as excavation and backfill after retaining walls [11–13], bridge abutments [14–17], pipeline and trench ducts [18], pavement bases [19–24], and so on. All these studies reflect requirement of the identification of mechanical constants of the CLSMs. Though it is known that the Young's modulus of CLSMs lies between soil and commonly used concrete, precise determination of engineering material properties of CLSMs (even for soil and concretes) is a questionable and difficult problem. For example, modulus of elasticity is evaluated by experiments using secant modulus of stress-strain curve or estimated from empirical formula of Young's modulus with 28-day compressive strength or weight of concrete.

Besides, artificial neural networks had been widely applied to various engineering [25], especially to civil and construction engineering [26, 27]. Alternately, several studies were conducted on the application of inverse problems in structural and geotechnical problems [28–32].

## 2. Problem definition and data preparation

### 2.1. Parameter recognition considered as inverse problem

In a classical mechanical analysis of civil engineering problems, we determinate displacements and/or stresses of a structure with known engineering constants, such as the Young's modulus,  $E$  (with the unit *GPa*), and the Poisson's ratio,  $\nu$ , which had been identified from laboratory or in-site experiments. This kind of problems can be termed *forward problems*, that is, we evaluate the unknown dependent variables (physical quantities) from prescribed parameters and dimensions analytically if there exist some closed-form relationships, or numerically using computational schemes (such as the finite element methods, FEMs) if the domain and/or boundary conditions are complicated.

On the other hand, an *inverse problem* in this case is to identify the engineering constants of a structure through evaluated or measured displacements and/or stresses. For a simple problem which can be analyzed and the results can be expressed in closed-form mathematical relationship, the inverse problem can be easily obtained from mathematical operation. However, for a practical huge structure of complicated shape, closed-form relationship cannot be obtained. Recently, a lot of schemes had been developed for parameter recognition (classification and regression) in the

Problem	Process	Problem with closed-form expression	Problem without closed-form expression
Forward	model parameters → model → prediction of data	$y = f(p_1)$ (e.g., $\Delta = \frac{PL^3}{3EI}$ )	parameters → numerical models (FEM) → displacements, stresses
Inverse	data → model → estimation of model parameters	$p_1 = f^{-1}(y)$ (e.g., $E = \frac{PL^3}{3I\Delta}$ )	displacements, stresses → welled trained ANNs → parameters

**Table 1.** Comparison of forward problem and inverse problem.

field of machine learning and artificial intelligence, among which neural networks such as back-propagation artificial neural network (BPANN) and radial basis function neural network (RBFNN) are proven to be powerful and efficient if well designed, trained, and tested.

The two problems are compared and illustrated in **Table 1**, where problems with and without closed-form relationship between parameters and physical quantities are shown, respectively. In **Table 1**, a well-known example in civil engineering, displacement at the end of a cantilevered beam subjected to a concentrated load is shown, in which  $\Delta, P, L, E, I$  denotes the end displacement, loading, length, Young’s modulus, and moment of inertia, respectively.

This research study aims to consider the identification of engineering constant of a typical CLSM-backfilled region as an inverse problem. The processes employed are as follows: (1) preparation of training data, and testing data through numerical analysis (using ANSYS); (2) preparation of verification data (from experiments on CLSMs); (3) normalization of training data, testing data, and verification data; (4) conducting prediction using neural networks of BPANN and RBFNN along with comparison study of parameters involved in the networks; and (5) selection of a useful network topology for parameter recognition.

In the following sections, the procedures are explained with numerical results.

## 2.2. Typical problem employed for the recognition of engineering constants

A typical problem of backfilled region after a retaining wall is considered (**Figure 1**). The length and height of backfilled region is  $L = 20 \text{ m}$ ,  $H = 5 \text{ m}$ , respectively. For simplicity, the

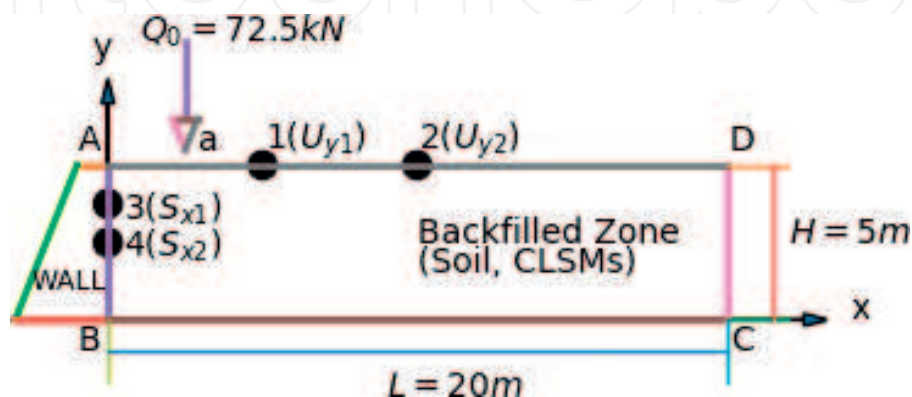


**Figure 1.** Schematic of a typical CLSM-backfilled region for the analysis of parameter recognition.

backfilled materials are considered to be linearly elastic and are within small deformation under external loadings; therefore, linear elastic analysis can be performed using only two engineering constants, that is, the Young's modulus,  $E$  (with the unit  $GPa$ ), and the Poisson's ratio,  $\nu$ . Furthermore, considering the width of backfilled zone is infinitely long, and a two-dimensional analysis can be used. In order to evaluate the engineering constants through displacements and stresses, the backfilled region is assumed to be subjected to a concentrated vertical loading (surcharge)  $Q_0 = 72.5 \text{ kN}$  acting at the point behind the retaining wall  $a = 0.5 H$ .

In order to provide training data and testing data in parameter recognition using neural networks, the following four quantities are defined:

$x_1 = U_{y1}$ : vertical displacement (settlement) at upper surface ( $x = L/4$ ), (positive downward,  $m$ ).

$x_2 = U_{y2}$ : vertical displacement (settlement) at upper surface ( $x = L/2$ ), (positive downward,  $m$ ).

$x_3 = S_{x1}$ : horizontal normal stress (lateral earth pressure) on wall ( $y = 3H/4$ ), (tensile positive,  $Pa$ ).

$x_4 = S_{x2}$ : horizontal normal stress (lateral earth pressure) on wall ( $y = H/2$ ), (tensile positive,  $Pa$ ).

These sampling points are illustrated in **Figure 1**.

### 2.3. FEM analysis using ANSYS

Finite element equation for elastic analysis of displacement and stress of a plane deformation problem can be expressed in matrix form [33]:

$$[K]\{X\} = \{F\} \quad (1)$$

where  $[K]$ ,  $\{X\}$ ,  $\{F\}$  denotes global stiffness matrix, global degrees of freedom vector and global load vector respectively, defined as follows:

$$[K] = \sum_{e=1}^{NE} [k]^e = \sum_{e=1}^{NE} t \iint_{A^e} [B]^T [D] [B] dx dy \quad (2)$$

$$\{F\} = \sum_{e=1}^{NE} \{f\}^e = \sum_{e=1}^{NE} t \oint_{S^e} [N]^T \{q\} dS$$

If a plane 4-node isoparametric element is used, the shape functions in Eq. (2) can be expressed as

$$\begin{aligned} N_1(\xi, \eta) &= (1 - \xi)(1 - \eta)/4 \\ N_2(\xi, \eta) &= (1 + \xi)(1 - \eta)/4 \\ N_3(\xi, \eta) &= (1 + \xi)(1 + \eta)/4 \\ N_4(\xi, \eta) &= (1 - \xi)(1 + \eta)/4 \end{aligned} \quad (3)$$

where  $\xi$ ,  $\eta$  are local coordinates. A typical PLANE42 element in ANSYS is shown in **Figure 2**.

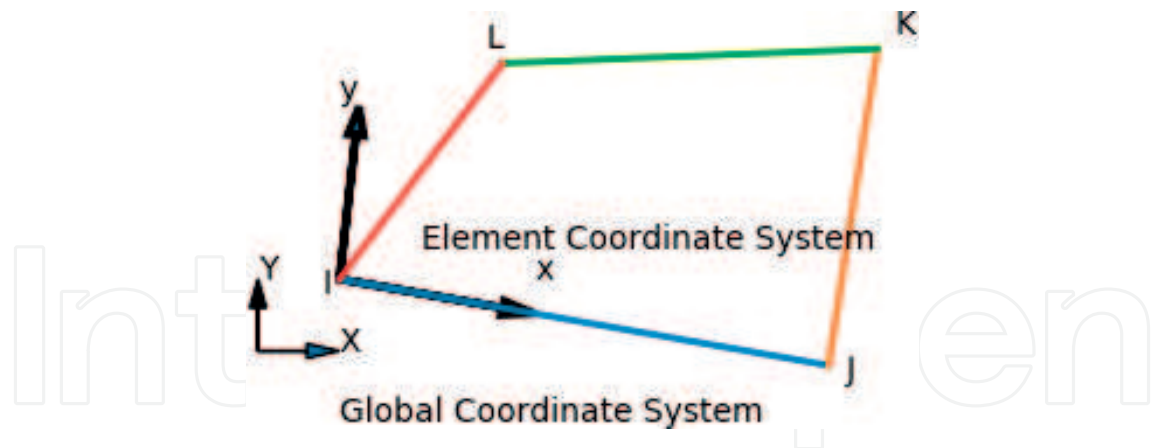


Figure 2. Definition of PLANE42 element of ANSYS [34].

#### 2.4. Numerical experiments for different combination of engineering constants

A finite element mesh with  $40 \times 10 = 400$  elements,  $41 \times 11 = 451$  nodes,  $451 \times 2 = 902$  degrees of freedom (displacements) is employed for a numerical analysis of backfilled zone (Figure 3). The left-hand side and right-hand side can only move freely in vertical direction, while the bottom of backfilled zone is considered fixed in both directions. In order to provide enough sampling data for later training and testing process using supervised neural networks, the Young's modulus ( $E$ ) ranges from 0.02 to 3 GPa (covering the general values of soil and

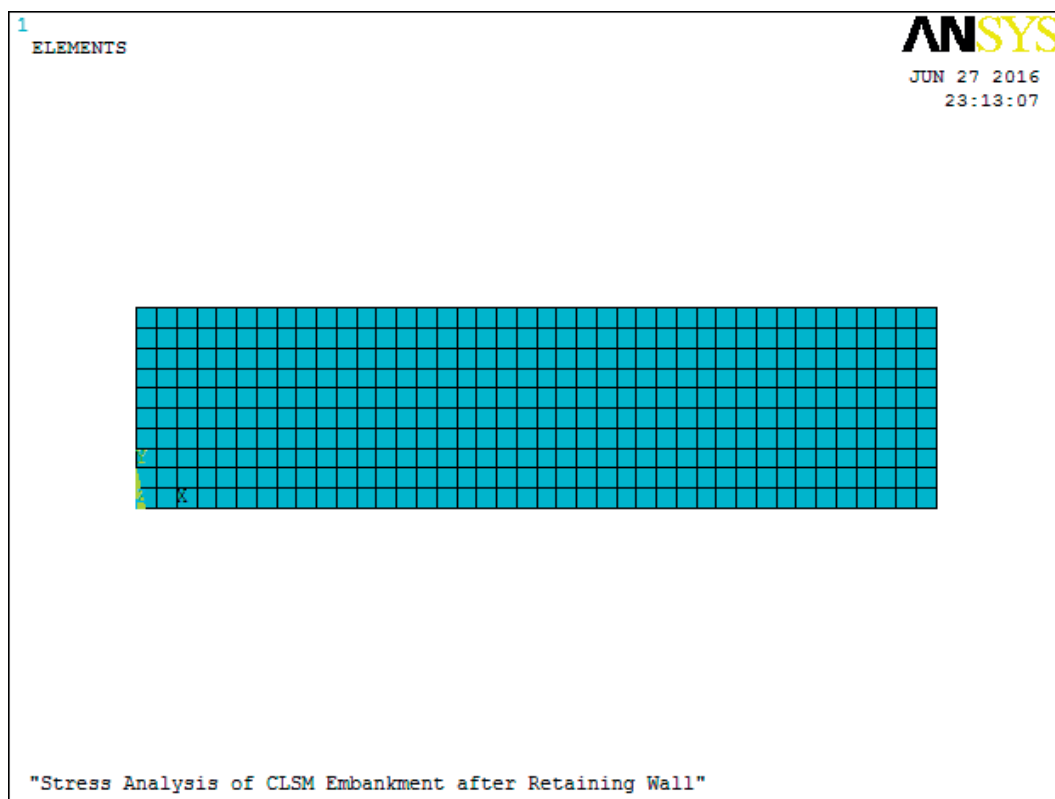


Figure 3. FEM mesh of the typical example of CLSM-backfilled region using ANSYS of PLANE42 elements.

CLSMS), while the Poisson's ratio ( $\nu$ ) is selected to be 0.1, 0.2, 0.25, 0.3, and 0.4. A total of 270 data samples with different combinations of  $E$  and  $\nu$  are used.

## 2.5. Data preparation

### 2.5.1. Data collection from FEM analysis using ANSYS

**Table 2** shows part of the 270 numerical results of computed displacements and stresses for different Young's moduli and Poisson's ratio using the ANSYS PLANE42 model.

### 2.5.2. Normalization of data

Since the output range of the sigmoid function is within  $[0, 1]$ , and in order to have a better performance of training of neural network, the input data should be normalized to have a uniformly ranged data.

The relationship between normalized and original data can be expressed as follows:

$$\begin{aligned}\tilde{x} &= a_x x + b_x \\ \tilde{y} &= a_y y + b_y\end{aligned}\quad (4)$$

where  $a_x, b_x$  are selected such that  $\tilde{x} \in [-1, 1]$ ,  $a_y, b_y$  are chosen to let  $\tilde{y} \in [0, 1]$ . In this case, the relations are

$$\begin{aligned}\tilde{x}_1 &= x_1/0.001 \\ \tilde{x}_2 &= x_2/0.001 \\ \tilde{x}_3 &= x_3/9000 \\ \tilde{x}_4 &= x_4/9000 \\ \tilde{y}_1 &= 3^* y_1/10^{10} \\ \tilde{y}_2 &= y_2\end{aligned}\quad (5)$$

Data	$x_1, U_{y1} (m)$	$x_2, U_{y2} (m)$	$x_3, S_{x1} (Pa)$	$x_4, S_{x2} (Pa)$	$y_1, E(GPa)$	$y_2, \nu$
1	-0.00098	1.9447E-05	-4452.6	-4029.1	0.02	0.1
2	-4.91E-04	9.72E-06	-4452.6	-4029.1	0.04	0.1
55	-0.0008607	2.6951E-05	-5434.05	-5196	0.02	0.2
56	-0.0004303	1.3476E-05	-5434.05	-5196	0.04	0.2
109	-7.61E-04	4.36E-05	-5979.35	-5862.9	0.02	0.25
110	-3.80E-04	2.18E-05	-5979.35	-5862.9	0.04	0.25
163	-0.62826E-03	0.72850E-04	-6567.6	-6599	0.02	0.3
164	-3.14E-04	3.64E-05	-6567.6	-6599	0.04	0.3
269	-1.88E-06	1.50E-06	-7896.55	-8337.1	2.5	0.4
270	-1.56E-06	1.25E-06	-7896.55	-8337.1	3	0.4

**Table 2.** Computed displacements and stresses for different Young's moduli and Poisson's ratio using the ANSYS PLANE42 model.

Data	$x_1, U_{y1} (m)$	$x_2, U_{y2} (m)$	$x_3, S_{x1} (Pa)$	$x_4, S_{x2} (Pa)$	$y_1, E(GPa)$	$y_2, \nu$
1	0.980000	0.019447	-0.494733	-0.447678	0.006000	0.100000
2	0.491200	0.009721	-0.494733	-0.447678	0.012000	0.100000
55	0.860680	0.026951	-0.603783	-0.577333	0.006000	0.200000
56	0.430340	0.013476	-0.603783	-0.577333	0.012000	0.200000
109	0.760910	0.043562	-0.664372	-0.651433	0.006000	0.250000
110	0.380450	0.021781	-0.664372	-0.651433	0.012000	0.250000
163	0.628260	0.072850	-0.729733	-0.733222	0.006000	0.300000
164	0.314130	0.036425	-0.729733	-0.733222	0.012000	0.300000
269	0.001876	0.001505	-0.877394	-0.926344	0.750000	0.400000
270	0.001564	0.001254	-0.877394	-0.926344	0.900000	0.400000

**Table 3.** Typical normalized FEM computed displacements and stress at sampling points.

Part of typical normalized FEM computed displacements and stress at sampling points are shown in **Table 3**. Among these normalized data, 216 set (216/270  $\cong$  80%) are selected randomly for training and 54 set (54/270  $\cong$  20%) for testing in the later neural work analyses.

### 2.5.3. Data for verification

In order to verify the trained and tested neural networks, three data set of backfilled materials are used: (1) the first is commonly used soil ( $E = 0.1 \text{ GPa}$ ,  $\nu = 0.30$ ); (2) CLSM-B80/30% ( $E = 0.27 \text{ GPa}$ ,  $\nu = 0.25$ ); and (3) CLSM-B130/30% ( $E = 0.87 \text{ GPa}$ ,  $\nu = 0.25$ ). The CLSM-B80/30% and CLSM-B130/30% denote unit weight of binder of the CLSM is 80 and 130  $\text{kg/m}^3$  with 30% of replacement of cement by fly ash. Selection of materials for the CLSM mixture in this study consisted of fine aggregate, type I Portland cement, stainless steel reducing slag (SSRS), and water. Fine aggregate for CLSM was formed by well blending between river sand and residual soil with a given proportion (e.g., 6:4, by volume) for grading improvement. The soil was obtained from a construction site. The experimental work was conducted on two binder content levels in mixtures (i.e., 80- and 130  $\text{kg/m}^3$ ). The water-to-binder ratio was selected via few trial mixes until the acceptable flowability for CLSM of 150–300  $\text{mm}$  was achieved. The detailed information can be seen in [8].

In **Table 4**, computed displacements and stresses for verified soil and two CLSMs using the ANSYS PLANE42 model are summarized, while the normalized data for verification are tabulated in **Table 5**.

Data	$x_1, U_{y1} (m)$	$x_2, U_{y2} (m)$	$x_3, S_{x1} (Pa)$	$x_4, S_{x2} (Pa)$	$y_1, E(GPa)$	$y_2, \nu$
Soil	-1.26E-04	1.46E-05	-6567.6	-6599	0.1	0.3
CLSM-B80/30%	-5.64E-05	3.23E-06	-5979.35	-5862.9	0.27	0.25
CLSM-B130/30%	-1.75E-05	1.00E-06	-5979.35	-5862.9	0.87	0.25

**Table 4.** Computed displacements and stresses for verified soil and two CLSMs using the ANSYS PLANE42 model.

Data	$x_1, U_{y1} (m)$	$x_2, U_{y2} (m)$	$x_3, S_{x1} (Pa)$	$x_4, S_{x2} (Pa)$	$y_1, E (GPa)$	$y_2, \nu$
Soil	-0.126	0.0146	-0.72973	-0.73322	0.003	0.3
CLSM-B80/30%	-0.0564	0.00323	-0.66437	-0.65143	0.0081	0.25
CLSM-B130/30%	-0.0175	0.001	-0.66437	-0.65143	0.0261	0.25

**Table 5.** Normalized FEM computed displacements and stress for verified soil and two CLSMs using the ANSYS PLANE42 model.

### 3. Parameter recognition using BPANN

#### 3.1. Application of BPANN for parameter recognition

**Figure 4** demonstrates a typical BPANN for the identification of engineering constants of CLSM. The BPANN shown in **Figure 4** contains a single output, that is, the Young's modulus ( $y_1 = E, y_2 = \nu$ ),  $L$  input neurons ( $x_i, i = 1, 2, \dots, L$ ), and  $M$  hidden neurons ( $h_j, j = 1, 2, \dots, M$ ). The predicted outputs can be expressed as [35–37]:

- a. from input layer (IL) to hidden layer (HL):

$$h_j = f(n_j) = f\left(\sum_{i=1}^L w_{ji} x_i - b_j\right) \quad (6a)$$

- b. from hidden layer (HL) to output layer (OL):

$$y_k = f(n_k) = f\left(\sum_{j=1}^M w_{kj} h_j - b_k\right) \quad (6b)$$

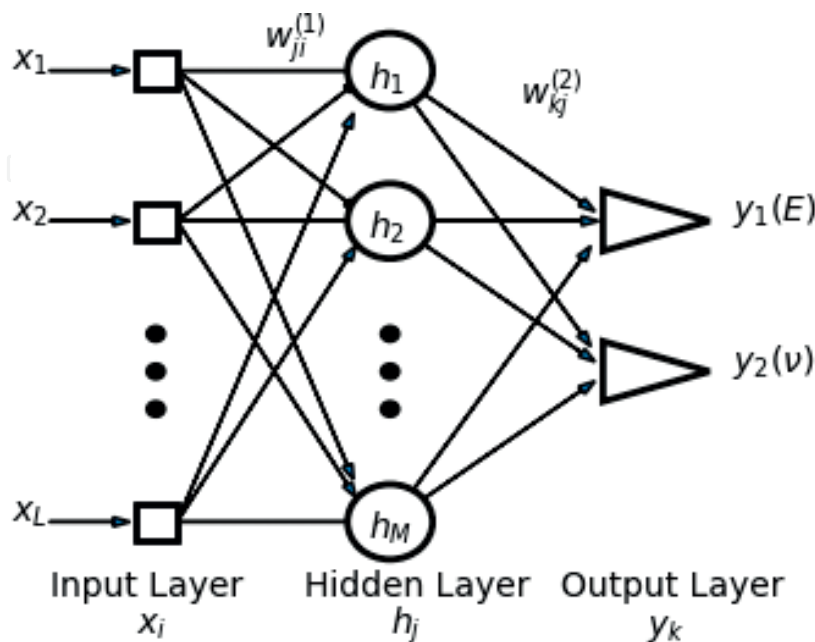


**Figure 4.** Schematic of a BPANN topology for single parameter recognition.

Where the activating function (the sigmoid function) and its derivative can be expressed as.

$$f(n) = \frac{1}{1 + e^{-n}} \tag{7}$$

$$f'(n) = f(n)[1 - f(n)].$$

### 3.2. Learning algorithms of BPANN for parameter recognition

There exist many approaches for the determination of the network parameters in BPANN ( $w_{kj}$ ,  $b_k$ ,  $w_{ji}$ ,  $b_j$ ). The most basic and popular generalized delta rule based on the method of the steepest descent along with two learning parameters (i.e., the learning rate  $\eta$  and the momentum factor  $\mu$ ) is employed, which can be expressed as

$$w_{kj}(p + 1) = w_{kj}(p) - \eta \frac{\partial E}{\partial w_{kj}}(p) + \mu w_{kj}(p)$$

$$b_k(p + 1) = b_k(p) - \eta \frac{\partial E}{\partial b_k}(p) + \mu b_k(p) \tag{8}$$

$$w_{ji}(p + 1) = w_{ji}(p) - \eta \frac{\partial E}{\partial w_{ji}}(p) + \mu w_{ji}(p)$$

$$b_j(p + 1) = b_j(p) - \eta \frac{\partial E}{\partial b_j}(p) + \mu b_j(p)$$

where

$$E(p) = \frac{1}{2} \sum_{k=1}^N e_k^2(p) = \sum_{k=1}^N \frac{1}{2} [d_k(p) - y_k(p)]^2 \tag{9}$$

denotes the error between targets and trained output results.

$$\frac{\partial E}{\partial w_{kj}}(p) = -e_k(p) f'(n_k) h_j$$

$$\frac{\partial E}{\partial b_k}(p) = -e_k(p) f'(n_k)^2$$

$$\frac{\partial E}{\partial w_{ji}}(p) = -\sum_{k=1}^N [e_k(p) f'(n_k) w_{kj}] f'(n_j) x_i \tag{10}$$

$$\frac{\partial E}{\partial b_j}(p) = -\sum_{k=1}^N [e_k(p) f'(n_k) w_{kj}] f'(n_j)$$

The MATLAB toolbox *nntool* provides a lot of training methods along with BPANN [38], among which four kinds of training algorithms were tested in the current research as follows:

**a. Generalized steepest decent (GD):**

The learning rule can be written as Eq. (8) with  $\eta \neq 0$ ,  $\mu = 0$ .

**b.** Generalized steepest decent including momentum (GDM):

The learning rule can be written as Eq. (8) with  $\eta \neq 0$ ,  $\mu \neq 0$ .

**c.** Generalized steepest decent with adjustable learning rate (GDA):

In this algorithm, the basic learning rule is the same as Eq. (6) but adding a conditional judgment. When stable learning can be kept under a learning rate, then the learning rate is increased, otherwise it is decreased. The learning rate increment and decrement can be denoted as  $\zeta_{inc}$  and  $\zeta_{dec}$  [35].

**d.** Levenberg-Marquardt (LM):

The learning rule can be written as

$$\Delta w_{ij}(t+1) = w_{ij}(t+1) - w_{ij}(t) = -\left[ [J]^T [J] + \lambda [I] \right]^{-1} [J]^T \{e\} \quad (11)$$

where  $\lambda$  denotes a constant to assure the inversion of matrix, and the learning rule becomes Gauss-Newton algorithm when  $\lambda = 0$ , while it approaches GD with small learning rate with large  $\lambda$  [35].

### 3.3. Numerical results of parameter recognition using BPANN

The first supervised learning employed for parameter recognition of engineering constants is the BPANN, which can be easily implemented for multiple inputs and multiple outputs. Since there are various design parameters in the construction of a BPANN, we study some influence factors (such as different algorithms of training rules, different combination of input variables, and number of neurons of hidden layer), and then we propose and analyze an appropriate topology of BPANN. The MATLAB nntool is used for network simulation.

#### 3.3.1. Comparison of different algorithms of learning rules

The convergence of RSME with iteration of BPANN by using different training algorithms under a BPANN topology with 4–6–2 (NI = 4, NH = 6, NO = 2) for the 216 training set is shown in **Figure 5**. The training functions in MATLAB are as follows: (1) GD (*traingd*); (2) GDM (*traingdm*); (3) GDA (*trainгда*); and (4) LM (*trainlm*). Some parameters employed in the four BPANN algorithms are also shown in **Figure 5**. It can be observed that except LM (*trainlm*), all another three algorithms cannot allow the root mean square errors (RMSEs) approach to zero quickly. (The results had been verified by the self-developed BPANN by using GD learning rule programming in Python). This reflects the current problem that contains a special feature that first-order method of the steepest decent cannot help to find the global minimum quickly, while the Levenberg-Marquardt (LM) algorithms based on Hessian matrix containing second-order derivative of cost function work well.

**Table 6** summarizes the effect of different training algorithms of BPANN on the predicted accuracy. It can be shown that LM (*trainlm*) gives accurate prediction of both the Young's modulus (error is within 6% for CLSMs) and Poisson's ratio (error is 1% for all) for three kinds of backfilled materials.

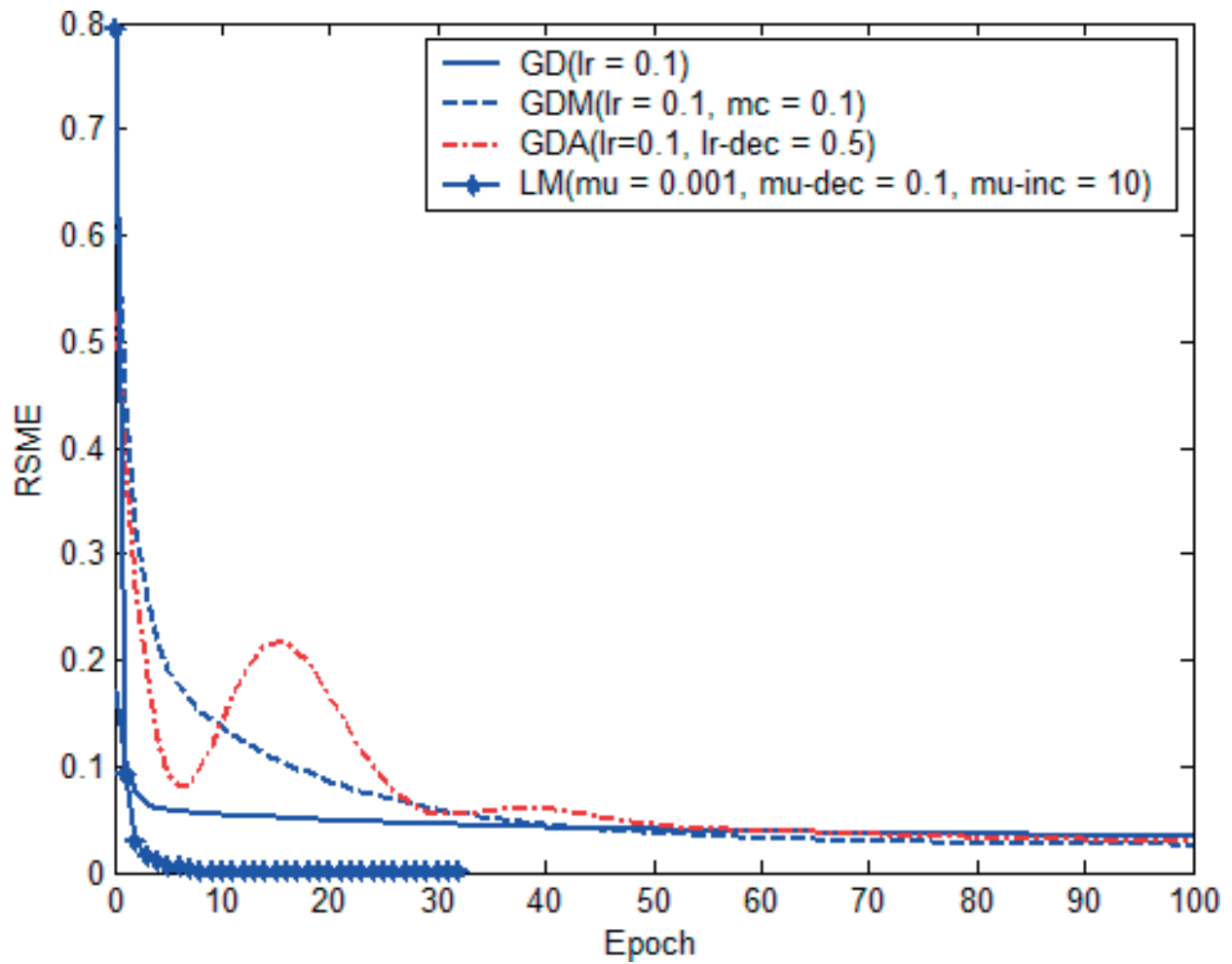


Figure 5. Convergence of RSME with iteration of BPANN using different training algorithms (NI = 4, NH = 6, NO = 2).

Case	Training method	RSME	Soil		CLSM-B80/30%		CLSM-B130/30%	
			E(Error%)	v(Error%)	E(Error%)	v(Error%)	E(Error%)	v(Error%)
1	<i>traingd</i>	0.02	0.5855 (485.5%)	0.4109 (36.95%)	0.6875 (154.6%)	0.2769 (10.75%)	0.7356 (-15.45%)	0.2717 (8.69%)
2	<i>traingdm</i>	0.02	0.5234 (423.4%)	0.3307 (10.24%)	0.6700 (148.2%)	0.2628 (5.11%)	0.6875 (-20.97%)	0.2581 (3.25%)
3	<i>traingda</i>	0.02	0.5148 (414.8%)	0.2181 (-27.30%)	0.5695 (110.92%)	0.1999 (-20.06%)	0.5766 (-33.72%)	0.2049 (-18.06%)
4	<i>trainlm</i>	0.00	<b>0.0729</b> (-27.11%)	<b>0.2991</b> (-0.31%)	<b>0.2862</b> (5.99%)	<b>0.2512</b> (0.49%)	<b>0.8561</b> (-1.60%)	<b>0.2510</b> (0.40%)
Experimental value			0.1	0.3	0.27	0.25	0.87	0.25

Table 6. Effect of different training algorithms of BPANN on the predicted accuracy.

### 3.3.2. Effects of input variable combinations

In a practical engineering situation, we are interested in a question: what physical variables should we measure? To solve this problem, five cases of different combination of input variables are investigated:

Case 1:  $(U_{y1}, U_{y2}, S_{x1}, S_{x2})$  (NI = 4) (two displacements, two stresses).

Case 2:  $(U_{y1}, U_{y2}, S_{x1})$  (NI = 3) (two displacements, one stress).

Case 3:  $(U_{y1}, U_{y2})$  (NI = 2) (two displacements).

Case 4:  $(U_{y1}, S_{x1})$  (NI = 2) (one displacement, one stress).

Case 5:  $(S_{x1}, S_{x2})$  (NI = 2) (two stresses).

The convergence of RSME with iteration of BPANN using different combinations of input variables using LM training algorithms (NH = 6, NO = 2) for the 216 training set is shown in **Figure 6**. Again, LM works well, but the predicted accuracy shown in **Table 7** depicts that only cases 1, 2, and 3 are appropriate for use. The result of case 5 reflects the fact that only stresses information cannot predict the material constant. Therefore, in the following analysis, we basically consider input variables of case 1; this means we need to measure two displacements and two stresses.

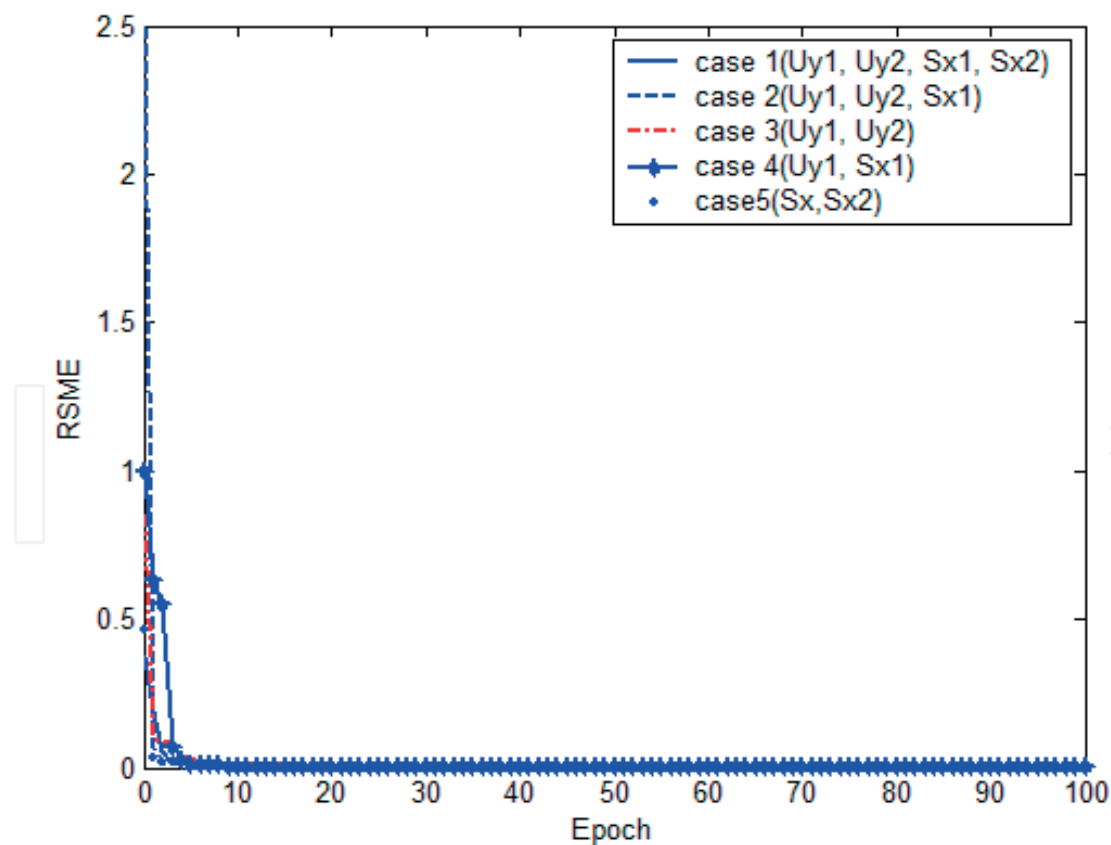


**Figure 6.** Convergence of RSME with iteration of BPANN using different combinations of input variables (trainlm, NI = 4, NH = 6, NO = 2).

Case	NI	Input variables	Soil		CLSM-B80/30%		CLSM-B130/30%	
			E(Error%)	v(Error%)	E(Error%)	v(Error%)	E(Error%)	v(Error%)
1	4	Uy1, Uy2, Sx1, Sx2	0.1363 (36.28%)	0.3003 (0.11%)	0.2368 (-12.30%)	0.2470 (-0.86%)	0.8636 (-0.73%)	0.2480 (-0.79%)
2	3	Uy1,Uy2, Sx1	0.0895 (-10.50%)	-0.2997 (-0.09%)	0.2795 (3.50%)	0.2518 (0.71%)	0.8618 (-0.95%)	0.2516 (0.65%)
3	2	Uy1, Uy2	0.0747 (-25.31%)	0.2997 (-0.10%)	0.2555 (-5.337%)	0.2501 (0.04%)	0.8485 (-2.48%)	0.2505 (0.21%)
4	2	Uy1, Sx1	7.5206 (7420%)	-0.1752 (-158.4%)	7.5706 (2704%)	-0.1768 (-17.7%)	7.6544 (779.8%)	-0.1724 (-168.9%)
5	2	Sx1, Sx2	1.3530 (1253%)	1.6716 (457.2%)	1.3079 (384.4%)	1.6449 (557.9%)	1.2985 (49.25%)	1.6331 (553.3%)
Experimental values			0.1	0.3	0.27	0.25	0.87	0.25

**Table 7.** Effect of input variables on the prediction accuracy of engineering constants using BPANN.

### 3.3.3. Effect of number of hidden neurons

The results of BPANN results using different number of neurons of hidden layer (NH) are shown in **Figure 7** and **Table 8**. From the results it is recommended to employ  $NH > 2$  for the accurate prediction of engineering constants if training algorithms LM (*trainlm*) are employed.

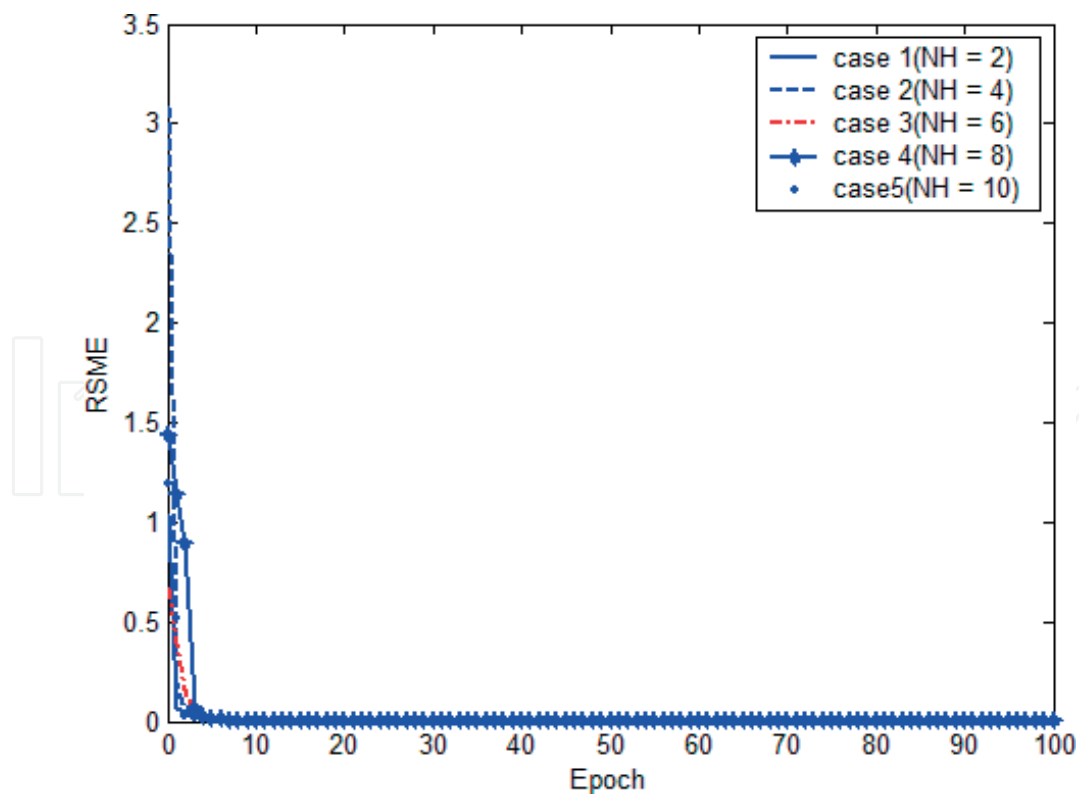


**Figure 7.** Convergence of RSME with iteration of BPANN using different number of neurons of hidden layer (*trainlm*, NI = 4, NO = 2).

Case	NH	NI-NH-NO	Soil		CLSM-B80/30%		CLSM-B130/30%	
			E(Error%)	v(Error%)	E(Error%)	v(Error%)	E(Error%)	v(Error%)
1	2	4-2-2-	0.2088 (108.80%)	0.3007 (0.22%)	0.2327 (-13.80%)	0.2498 (-0.08%)	0.9413 (8.20%)	0.2499 (-0.04%)
2	4	4-4-2	0.1562 (56.19%)	0.2878 (-4.06%)	0.3097 (14.69%)	0.2453 (-1.87%)	0.8903 (2.33%)	0.2498 (-0.09%)
3	6	4-6-2	0.1653 (65.35%)	0.2985 (-0.50%)	0.3238 (19.94%)	0.2491 (-0.36%)	0.8859 (1.83%)	0.2492 (-0.31%)
4	8	4-8-2	0.0811 (-11.91%)	0.3015 (0.51%)	0.2392 (-11.43%)	0.2507 (0.29%)	0.8566 (-1.54%)	0.2508 (0.34%)
5	10	4-10-2	0.1174 (17.39%)	0.2992 (-0.28%)	0.2777 (2.86%)	0.2531 (1.23%)	0.8833 (1.53%)	0.2542 (1.69%)
Experimental values			0.1	0.3	0.27	0.25	0.87	0.25

**Table 8.** Effect of number of neurons of hidden layer on the prediction accuracy of engineering constants using BPANN.

### 3.3.4. Selection of a BPANN topology

After some parametric studies, a BPANN with 4-6-2 topology using LM training algorithm is proposed for current parameter recognition problems. The convergence of RMSE is shown in **Figure 8** to depict very fast decay of RSME. **Figure 9** shows the QQ plot of tested results and predicted results during testing stage after training process. The  $R^2$  value for the Young's modulus and Poisson's ratio are 0.99454 and 0.99864, respectively. It reflects that the training

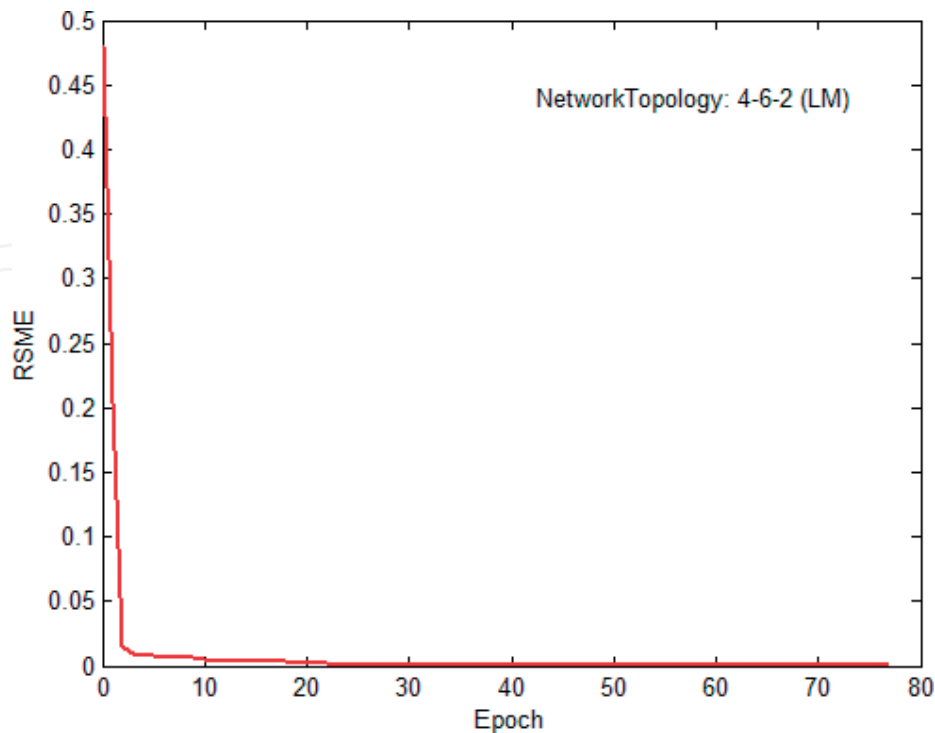


**Figure 8.** Convergence of RSME with iteration of finally selected of BPANN (trainlm, NI = 4, NH = 6, NO = 2).

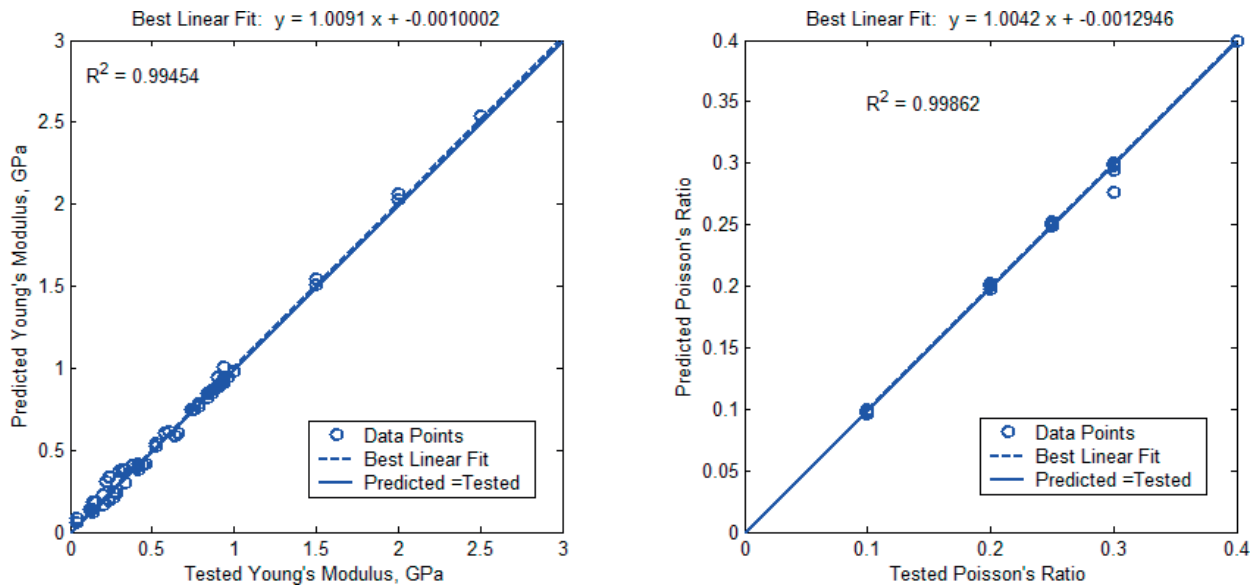


Figure 9. QQ plot of testing data of finally selected of BPANN (trainlm, NI = 4, NH = 6, NO = 2).

Training method	Input variables	NI-NH-NO	Soil		CLSM-B80/30%		CLSM-B130/30%	
			E(Error%)	v(Error%)	E(Error%)	v(Error%)	E(Error%)	v(Error%)
trainlm	Uy1, Uy2, Sx1, Sx2	4-6-2-	0.0729 (-27.11%)	0.2991 (0.31%)	0.2862 (5.99%)	0.2512 (0.49%)	0.8561 (-1.60%)	0.2510 (0.40%)
Experimental values			0.1	0.3	0.27	0.25	0.87	0.25

Table 9. Predicted results using final design of a BPANN for the recognition of engineering constants of CLSM.

BPANN works well for testing data. Table 9 shows predicted results using final design of a BPANN for the recognition of engineering constants of CLSM.

## 4. Parameter recognition using RBFNN

### 4.1. Application of RBFNN for parameter recognition

Figure 10 demonstrates a typical RBFNN for the identification of engineering constants of CLSM. The RBFNN shown in Figure 10 contains a single output, that is, the Young's modulus ( $y_1 = E$ ,  $y_2 = \nu$ ),  $L$  input neurons ( $x_i$ ,  $i = 1, 2, \dots, L$ ), and  $M$  hidden neurons ( $h_j$ ,  $j = 1, 2, \dots, M$ ). Suppose we have  $S$  samples for training, we can select  $M \leq S$ . The predicted output can be expressed as [35–37]:

$$y_k = F_k(x_i) = \sum_{j=1}^M w_j K(\|x_i - C_j\|) = \sum_{j=1}^M w_j e^{\frac{-1}{2\sigma_j^2} \|x_i - C_j\|^2} \quad (12)$$

where the kernel function  $K(\|x_i - C_j\|) = e^{\frac{-1}{2\sigma_j^2} \|x_i - C_j\|^2}$  is the Gaussian basis function.

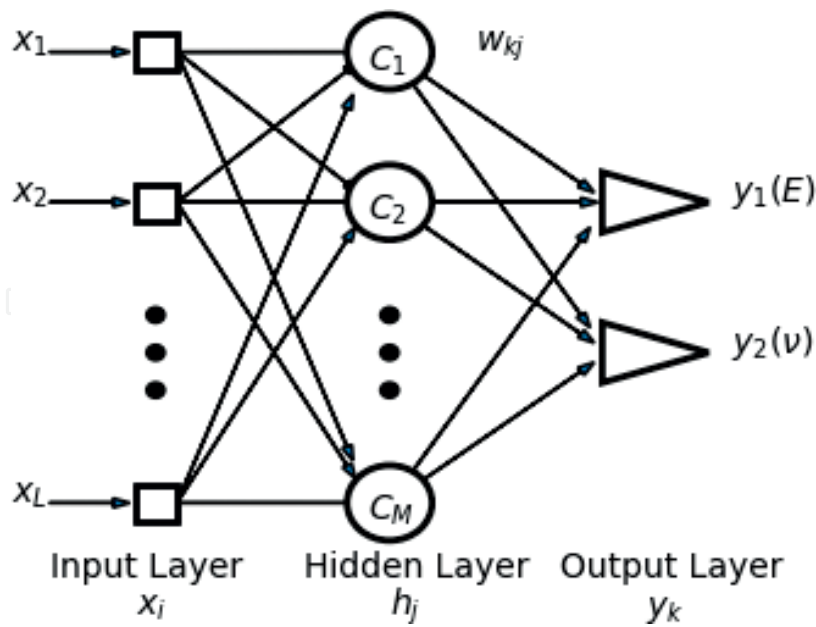


Figure 10. Schematic of a RBFNN topology for single parameter recognition.

#### 4.2. Learning algorithms for RBFNN for parameter recognition

There exist many approaches for the determination of the network parameters in RBFNN ( $C_j, \sigma_j, w_{kj}$ ). For parallel comparison, here the supervised learning algorithm, that is, the generalized delta rule based on the method of the steepest descent is used, which can be expressed as [35–37]:

$$\begin{aligned}
 w_{kj}(p + 1) &= w_{kj}(p) - \eta \frac{\partial E}{\partial w_{kj}}(p) + \mu w_{kj}(p) \\
 C_j(p + 1) &= wC_j(p) - \eta \frac{\partial E}{\partial C_j}(p) + \mu C_j(p) \\
 \sigma_j(p + 1) &= \sigma_j(p) - \eta \frac{\partial E}{\partial \sigma_j}(p) + \mu \sigma_j(p)
 \end{aligned}
 \tag{13}$$

where

$$E(p) = \frac{1}{2} \sum_{k=1}^N e_k^2(p) = \frac{1}{2} \sum_{k=1}^N [d_k(p) - y_k(p)]^2
 \tag{14}$$

denotes the error between targets and trained output results.

$$\begin{aligned}
 \frac{\partial E}{\partial w_{kj}}(p) &= -K(\|x_i(p) - C_j(p)\|) \\
 \frac{\partial E}{\partial C_j}(p) &= -w_{kj}(p) \frac{1}{\sigma_j^2(p)} K(\|x_i(p) - C_j(p)\|) \cdot [x_i(p) - C_j(p)] \\
 \frac{\partial E}{\partial \sigma_j}(p) &= -w_{kj}(p) \frac{1}{\sigma_j^3(p)} K(\|x_i(p) - C_j(p)\|) \cdot \|x_i(p) - C_j(p)\|^2
 \end{aligned}
 \tag{15}$$

There also exist many algorithms for learning RBFNN; among those, some are unsupervised ones such as using kNN for determination of  $C_j$  and using the pseudo-inversion method to evaluate  $w_{kj}$  [35–37].

### 4.3. Numerical results of parameter recognition using RBFNN

**Table 10** summarizes the accuracy of predicted results by using RBFNN with different combinations of input variables. MATLAB *nntool* (*newrb*) is used for numerical experiments [38]. Unfortunately, the results are not as good as those obtained using BPANN with the LM training method. **Figure 11** also reflects the same results that Young’s modulus cannot be

Case	NI	Input variables	Soil		CLSM-B80/30%		CLSM-B130/30%	
			E(Error%)	v(Error%)	E(Error%)	v(Error%)	E(Error%)	v(Error%)
1	4	Uy1, Uy2, Sx1, Sx2	0.1877 (87.73%)	0.3009 (0.30%)	0.5786 (114.29%)	0.2498 (-0.08%)	0.8085 (-7.07%)	0.2498 (-0.08)
2	3	Uy1,Uy2, Sx1	0.1649 (64.85%)	0.300 (0.00%)	0.5561 (105.95%)	0.2486 (-0.55%)	0.7832 (-9.98%)	0.2487 (-0.53%)
3	2	Uy1, Uy2	0.2124 (112.44%)	0.2151 (-28.31%)	0.5809 (115.15%)	0.2309 (-7.63%)	0.7983 (-8.25%)	0.2549 (1.98%)
4	2	Uy1, Sx1	0.1774 (77.44%)	0.3001 (0.02)	0.5072 (87.85%)	0.2450 (-2.01%)	0.7017 (-19.34%)	0.2425 (-3.00%)
5	2	Sx1, Sx2	0.6023 (502.27%)	0.300 (0.00)	0.6365 (135.74%)	0.2500 (0.01%)	0.6365 (-26.84%)	0.2500 (0.01%)
Experimental values			0.1	0.3	0.27	0.25	0.87	0.25

**Table 10.** Effect of input variables on the prediction accuracy of engineering constants using RBFNN.

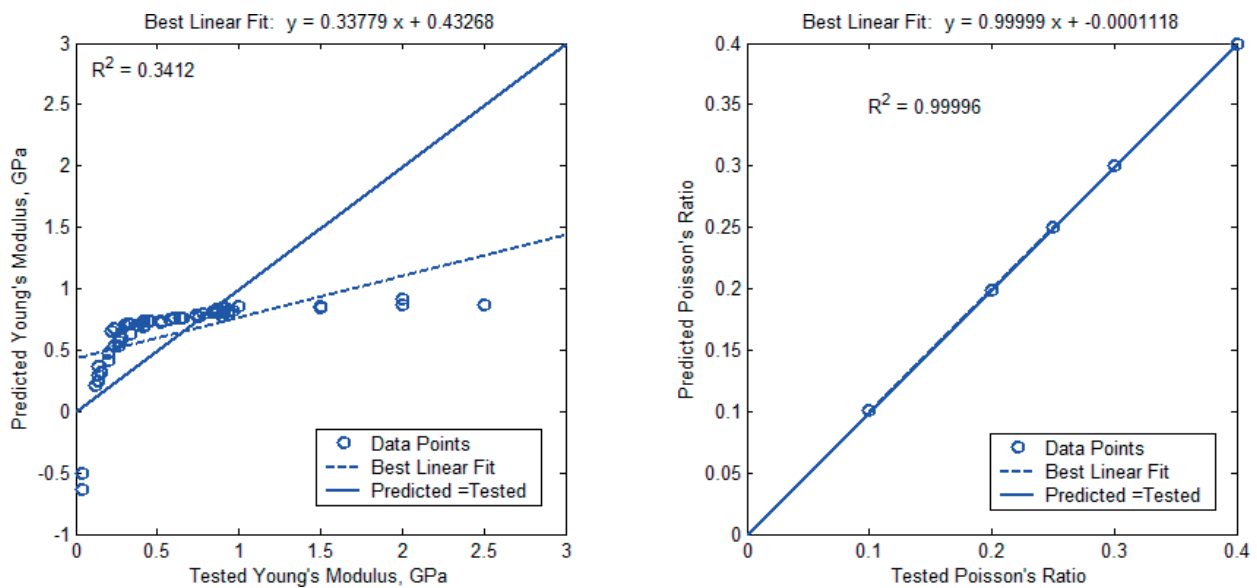


**Figure 11.** QQ plot of predicted and tested engineering constants of CLSM using RBFNN (NI = 4).

predicted well using RBFNN (even though a lot of trials on selection of spread constants cannot obtain satisfying results).

## 5. Conclusions

This chapter presents a trial of application of two supervised learning artificial neural networks (BPANN and RBFNN) to predict engineering material constants, Young's modulus and Poisson's ratio, of backfilled materials (soil and CLSMs). The training and testing data are obtained from numerical experiments using ANSYS. Concluding remarks can be summarized as follows:

1. BPANN with training method LM (such as `trainlm` in MATLAB) works well for parameter recognition of engineering constant. For example, a well-designed BPANN with LM (*trainlm*) can give accurate prediction of both Young's modulus (error is within 6% for CLSMs) and Poisson's ratio (error is with 1% for all) for three kinds of backfilled materials;
2. In the BPANN framework, at least two displacements at different points should be measured, together with optional 0, 1, or 2 stress measurements;
3. In the BPANN structure, for example, small number of neurons of hidden layer is enough for parameter recognition;
4. RBFNN is not appropriate for the parameter recognition of engineering constants, for example, as compared with BPANN.

In future, another neural network which is appropriate for regression, such as probabilistic neural networks (PNN) and supporting vector machines (SVM), maybe used for the study on the parameter recognition of engineering constants of problems in civil engineering.

## Author details

Li-Jeng Huang

Address all correspondence to: [ljhuang@kuas.edu.tw](mailto:ljhuang@kuas.edu.tw)

Department of Civil Engineering, National Kaohsiung University of Applied Sciences, Taiwan, R. O. C

## References

- [1] ACI-229R. Controlled-Low Strength Materials (Reproved 2005). Farmington Hills, MI, USA: American Concrete Institute (ACI); 2005.

- [2] Lachemi M, Şahmaran M, Hossain KMA, Lotfy A. Properties of controlled low-strength materials incorporating cement kiln dust and slag. *Cement and Concrete Composites*. 2010;**32**:623-629
- [3] Finney AJ, Shorey EF, Anderson, J. Use of native soil in place of aggregate in controlled low strength material (CLSM), International pipelines conference 2008 Atlanta, Georgia, United States, 2008; 1–13
- [4] Howard A, Gaughan M, Hattan S, Wilkerson M. Lean, green, and mean: The IPL Project. International Conference on Sustainable Design, Engineering, and Construction 2012 (ICSDEC 2012), November 7-9, 2012. Fort Worth, Texas, United States: ASCE. 2013;**1**:359-366
- [5] Huang LJ, Wang HY, Wei CT. Engineering properties of controlled low strength desulfurization slags (CLSDS). *Construction and Building Materials*. 2016;**115**:6-12
- [6] Huang LJ, Wang HY, Wu YY. Properties of the mechanical in controlled low-strength rubber lightweight aggregate concrete (CLSRLC). *Construction and Building Materials*. 2016;**112**:1054-1058
- [7] Huang LJ, Wang HY, Wang SYA. Study of the durability of recycled green building materials in lightweight aggregate concrete. *Construction and Building Materials*. 2015;**96**:353-359
- [8] Sheen YN, Huang LJ, Le DH. Engineering properties of controlled low-strength material made with residual soil and class F fly ash, 3rd International conference for advanced materials design and mechanics and workshop on android robotics, paper no. 54, Singapore, May 23–24, 2014
- [9] Huang LJ, Sheen YN, Le DH. On the multiple linear regression and artificial neural networks for strength prediction of soil-based controlled low-strength material, 3rd international conference for advanced materials design and mechanics and workshop on android robotics, paper no. 55, Singapore, May 23–24, 2014
- [10] Sheen YN, Hsiao DH, Huang LJ, Le DH. Stress-strain behavior of soil-based controlled low-strength material, The International Conference on Green Technology for Sustainable Development 2014, Ho Chi Minh, Viet Nam, October 30–31 2014
- [11] Alizadeh V, Helwany S, Ghorbanpoor A, Sobolev K. Design and application of controlled low strength materials as a structural fill. *Construction and Building Materials*. 2014;**53**: 425-431
- [12] Huang LJ, Sheen YN, Hsiao DH, Le DH. Numerical analysis of excavation backfilled with soil-based controlled low-strength materials: Part I- static analysis. *IJETAE*. 2014;**4**(12):132-139
- [13] Huang LJ, Sheen YN, Hsiao DH, Le DH. Numerical analysis of excavation backfilled with soil-based controlled low-strength materials: Part II- steady state elastodynamic analysis. *IJETAE*. 2014;**4**(12):140-148
- [14] Helwany S, Ghorbanpoor A, Alizadeh V, Oliva MA. Novel Abutment Construction Technique for Rapid Bridge Construction: CLSM with Full-Height Concrete Panels. DTRT06-G-0020,

National Center for Freight and Infrastructure Research and Education (CFIRE). University of Wisconsin-Madison; January, 2012

- [15] Schmitz ME, Parsons RL, Ramirez G, Zhao Y. Use of Controlled Low-Strength Material as Abutment Backfill. Technical report K-TRAN: KU-02-6, the Kansas Department of Transportation, Topeka, Kansas, University of Kansas, USA, June 2004
- [16] Huang LJ, Sheen YN, Le DH. Numerical analysis of controlled low-strength material bridge abutments: Part-I: Static analysis. The eighth structural engineering and construction conference (ISEC-8), Sydney, Australia, November 23–28, 2015
- [17] Huang LJ, Sheen YN, Le DH. Numerical analysis of controlled low-strength material bridge abutments: Part-II: Steady-state elasodynamic analysis. The eighth structural engineering and construction conference (ISEC-8), Sydney, Australia, November 23–28, 2015
- [18] Huang LJ, Wang HY, Sheen YN, Le DH. Earth pressure and settlement analysis of trench ducts backfilled with controlled low-strength materials. *Procedia Engineering*. 2016;142: 173-180
- [19] Lin DF, Luo HL, Wang HY, Hung MJ. Successful application of clsm on a weak pavement base/subgrade for heavy truck traffic. *Journal of Performance of Constructed Facilities*. 2007:70-77
- [20] Bassani M, Khosravifar S, Goulias DG, Schwartz CW. Long-term resilient and permanent deformation behavior of controlled low-strength materials for pavement applications. *Transportation Geotechnics*. 2015;2:108-118
- [21] Huang LJ, Wang HY, Huang WL, Lin MC. Finite element analysis of controlled low strength material pavement bases: Part-I: Static analysis. Resilient structures and sustainable construction. 9th International Conference in Structural Engineering and Construction. (ISEC-9), Valencia, Spain, July 24–29, 2017
- [22] Huang LJ, Wang HY, Huang WL, Lin MC. Finite element analysis of controlled low-strength material pavement bases: Part-II: Free vibration analysis. Resilient structures and sustainable construction. 9th International Conference in Structural Engineering and Construction. (ISEC-9), Valencia, Spain, July 24–29, 2017
- [23] Huang WL, Wang HY, Huang LJ. Viscoelastic analysis of flexible pavements embedded with controlled low-strength material bases using finite element method. The 2nd International Conference on Mechanics, Materials and Structural Engineering (ICMMSE 2017). Beijing, April 14-16, 2017
- [24] Tu TW, Wang HY, Huang LJ. Finite element analysis of cracked flexible pavements embedded with controlled low-strength material bases. The 2nd International Conference on Mechanics, Materials and Structural Engineering (ICMMSE 2017). Beijing, April 14-16, 2017

- [25] Oludele A, Olawale J. Neural networks and its application in engineering. Proceedings of Informing Science & IT Education Conference (InSITE). 2009
- [26] Kapania RK, Liu Y. Applications of artificial neural networks in structural engineering with emphasis on continuum models. Department of Aerospace and Ocean Engineering, Virginia Polytechnic Institute and State University Blacksburg, VA, USA
- [27] Jaina M, Pathak KK. Applications of artificial neural network in construction engineering and management-a review. International Journal of Engineering Technology, Management and Applied Sciences. 2014;2(3):134-142
- [28] Elshafiey I. Neural Network Approach for Solving Inverse Problems, MS thesis. Department of Electric Engineering and Computer Engineering, Iowa State University; 1991
- [29] Raiche A. Pattern recognition approach to geophysical inversion using neural nets. Geophysics Journal International. 1991;105(6):692-698
- [30] Li S-J, Liu Y-X, Zhang Z-P, Huang W, Shen G-H. Parameter identification of concrete dam with neural networks. Proceedings of Da-Lien University of Science and Engineering. 2000;40(5):531-535 (in Chinese)
- [31] Li S-J, Liu Y-X, Liu Y-J. Identification of elastic parameters of rock body in slope based on improved BP neural networks. Proceedings of College of Xian-Tan Mineral Engineering. 2002;17(1):58-61 (in Chinese)
- [32] Chang R-C, Ru E-L, Jien K-L. Modern Computational Mechanics, Chapter 10. In: Artificial Neural Networks and their Applications to Mechanics. Tsung-Chin University Press; 2004
- [33] Movaveni S. Finite Element Analysis: Theory and Application with ANSYS. Prentice Hall, Upper Saddle River, NJ, USA; 1999
- [34] ANSYS User's manual: Elements, Vol. III. Canonsburg, PA, USA: Swanson Analysis Systems, Inc; 1999
- [35] Hagen MT, Dmuth HB, Deale M. Neural Network Design. Boston, MA, USA: PWS Publishing Co.; 1996
- [36] Jang J-SR, Sun CT, Mizutani E. Neuro-Fuzzy and Soft Computing-A Computational Approach to Learning and Machine Intelligence, Chapter 9. Prentice-Hall, Upper Saddle River, NJ, USA; 1997
- [37] Haykin S. Neural Networks and Learning Machines. 3rd ed. Upper Saddle River, NJ, USA: Pearson Education, Inc; 2009 Chapter 4, Chapter 5
- [38] Neural Networks Toolbox User's Guide, The MathWorks, MA, USA; 2002

